Solid State Deuteron NMR Studies of Polyamidoamine Dendrimer Salts. 2. Relaxation and Molecular Motion

Dariya I. Malyarenko,[†] Robert L. Vold,*[,†] and Gina L. Hoatson[‡]

Departments of Applied Science and Physics, The College of William and Mary, P.O. Box 8795, Williamsburg, Virginia 23187-8795

Received May 25, 2000; Revised Manuscript Received July 28, 2000

ABSTRACT: Nonexponential recovery curves have been obtained for anisotropic deuteron spin lattice relaxation of deuterated polyamidoammonium chloride salts for integer generations $G = 1$, 2, 3, 5, 7, and 9, at room temperature. The temperature dependence of the relaxation of generations 2, 3, and 9 is reported. Multiple exponential relaxation behavior is ascribed to a sum of single exponential, anisotropic contributions from overlapping quadrupole echo powder patterns. These are assigned to interior secondary amide, R_2ND, deuterated tertiary amine, R_3ND^+, and terminal ammonium, RND_3^+, deuterons in the glassy polymer. Additional temperature dependent features in the middle of the spectra arise from mobile phases. For each type of deuteron the best fit of the relaxation data is achieved by numerically solving the stochastic Liouville equation for the relevant motional model. Planar libration of R_2ND and R_3ND^+ deuterons is simulated by jumps along an arc. Motion of RND_3^+ groups is modeled as a two-frame process in which ND_3^+ rotation proceeds at by jumps about the pseudo 3-fold R−N bond axis, which in turn jumps at among sites in a cone. Low, intermediate and high generation subclasses of solid dendrimers are defined on the basis of rates and activation energies for libration and rotation of their spacer groups, branch points, and termini. There are two superimposed powder patterns for terminal ammonium deuterons, distinguished only by their different relaxation behavior. These arise from fast (10^{10} s^{-1}) and slow (10^9 s^{-1}) ammonium rotors. For low and high generations, the fast rotors represent a small fraction (<30% at ambient temperature) of less constrained ammonium groups. With increasing temperature, the fraction of fast rotors decreases for G2 and G9, but increases for G3. Data reported here quantify a model in which dendrimer arms of G3 are neither extensively interpenetrated (as for G2) nor backfolded (as for G9).

1. Introduction

The growing scientific and industrial interest in regular three-dimensional synthetic polymers[1] has stimulated many investigations of dendrimer structure and dynamics.[2−10] Among the first representatives of regular hyperbranched polymers are the polyamidoamine (PAMAM) dendrimers, also termed "starburst" dendrimers to reflect the starlike symmetry of their growth.[11] Starburst dendrimers can be grown from ammonia or diamine cores. Their branches are composed of different length alkyl chains, with amide connectivity to the next tertiary amine branching site. Generation growth implies the addition of new chain-spacer units to terminal branching sites. The composition and the length of the spacers is the same at each polymerization step. Thus, essentially monodisperse polymeric material can be obtained if all terminal groups are involved in the growth reaction.[1]

Because of their very narrow molecular size distributions, dendrimers can be characterized more precisely than most linear polymers. However, the fractallike dendrimer architecture lacks long-range order and therefore cannot be investigated by crystallographic techniques. Solid-state nuclear magnetic resonance (NMR) provides a powerful combination of experimental techniques for this purpose. In particular, deuteron relaxation studies are distinguished by sensitivity to a wide range of motional rates, ranging from seconds to picoseconds.[12−14] Structural transitions in dendrimers and other polymers are naturally accompanied by changes in the amplitudes and rates of molecular motion.[12,15−17] Deuteron relaxation is an excellent choice of technique to quantitatively characterize these dynamical processes.

Quadrupole echo line shape analysis for deuterated PAMAM salts,[18] provided evidence of thermally activated planar librational motion in the dendrimer spacers and branching points, and a composite, two-frame motion of ammonium termini, RND_3^+. These motions compete with the stabilizing influence of hydrogen bonds at interior amide (R_2ND) and deuterated tertiary amine (R_3ND^+) sites. The balance between these competing trends was investigated and revealed a progression from the open, interpenetrated structures of low generation dendrimers to more symmetric, backfolded molecular architecture for high generations.

This paper quantifies the rates and activation energies of internal dendrimer motions (librations and rotation) on the basis of anisotropic, temperature-dependent T_{1Z} and T_{1Q} relaxation data. The analysis is complicated by the presence of overlapping powder patterns originating from unselective deuteron labeling. However, such labeling is easy to implement and has the benefit that a single experiment provides information on chemically and spatially different sites simultaneously. The approach developed here for analysis of relaxation data may be useful for other unselectively labeled materials with relatively narrow distributions of structural and dynamical parameters.

* To whom correspondence should be addressed, e-mail: rlv@nmr.physics.wm.edu.
[†] Department of Applied Science, The College of William and Mary.
[‡] Department of Physics, The College of William and Mary.

10.1021/ma000921u CCC: $19.00
Published on Web 09/13/2000

Results reported in this paper provide a definition of three dendrimer subclasses: low, intermediate, and high generation, on the basis of local segmental dynamics in solid, glassy materials. Low generation (G2) PAMAM dendrimer salts have segmental dynamics similar to those of high generation (G9) materials but are more extensively plasticized by protonation at the branching sites. Surface crowding without extensive backfolding is characteristic of intermediate (G3) dendrimer salts, and in the solid, this facilitates the formation an extensive intermolecular network of hydrogen-bonded termini. This unique behavior of solid, intermediate generation dendrimers has a counterpart in solution, where a well-known transition occurs from unfolded, open structures at low generation to globular, backfolded morphology for high generation dendrimers. For solid, high generation ($G > 3$) dendrimer salts, the arms are deeply backfolded and span the dendrimer interior to the same extent as the interpenetrated arms of low generations. In contrast to theoretical predictions of ref 19, but in agreement with kinetic growth models,[20] the generation dependence of segmental chain dynamics revealed by deuteron NMR does not support the existence of a dense surface shell for high generation materials. In general, hydrogen bonding in PAMAM dendrimers strongly affects activation energies for spacer and branch site libration.

In glassy linear polymers, librational motion (especially above T_g) is usually characterized by a broad distribution of rates, this leads to characteristically nonexponential spin relaxation recovery curves. We have attempted to fit the relaxation data for solid PAMAM dendrimers to this type of model without success. Instead, the anisotropy of relaxation observed for overlapping powder patterns can readily be fit by associating a single motional process with at most narrow distributions of rates for spacer, branch, and terminal sites, respectively. This unusual behavior of solid dendrimers is presumably associated with the packing of highly branched arms. In solution, where the solvent imparts greater mobility to chain ends, distributions of motional rates are expected and observed.[2,3]

2. Experimental Methods

Material Preparation. Salt preparation from amine terminated diamine core dendrimer generations 1, 2, 3, 5, 7, and 9 and deuteron exchange reactions followed by solvent removal were performed in four steps as described previously.[18] At each deuteration step, chemical exchange in D_2O solution was allowed to proceed for at least 12 h to ensure equilibration, followed by drying under nitrogen at 60 °C for 24 h. After a second exchange with D_2O, samples were dried under vacuum for 3 days. It is possible that this is not sufficient to remove all solvent,[21] but the contribution of residual solvent (methanol, hydrochloric acid and water) deuterons is not large enough to interfere with the data analysis. Excess DCl in solution should result in complete deuteration of interior tertiary amine branching sites in addition to the ammonium termini.[22] However, the extent of deuteration was not controlled and it is possible that some sites lose deuterons during solvent removal. Deuteration at low acid concentrations, at least for low generation materials, can be expected to occur predominantly at branching sites two spacers apart due to effects of electrostatic repulsion.[22] Thus, it is possible that deuteration occurs in part "by layers" (e.g., at termini and at generation 0 sites for G2), and for high generation dendrimers, the layers accessible might not extend into the dendrimer core.

Measurements. Experimental instrumentation and sample handling procedures were the same as described previously.[18] Quadrupole echo spectra and relaxation measurements were carried out at 46 MHz using a home-built spectrometer. The dried materials are extremely hygroscopic. NMR samples were packed and sealed under dry nitrogen and were kept in a drybox between measurements. On the basis of literature citations[15,16,23−26] and our experimental results,[18] the overlapping powder patterns observed for all dendrimer generations are assigned to deuterons at spacer secondary amide sites, R_2ND, deuterated branching tertiary amine sites, R_3ND^+, and terminal ammonium, RND_3^+, sites.[18] Small isotropic peaks are observed in the middle of the spectrum, at temperatures approaching the very broad glass transition region.[18]

In the powder patterns, deviations of the integrated relative intensities from calculated values (based on the known stoichiometry[18]) arise, in part, from incomplete deuteration at the branching sites. This would be expected if, as noted above, the deuteration of interior sites proceeds by layers. If the amplitude of spacer R_2ND librational motion of the branches attached to undeuterated R_3N sites is significantly smaller than that on branches involving R_3ND^+ sites, secondary amide deuterons on the former could go undetected because of very long relaxation times[16] (>100 s). Experimental quadrupole echo spectra obtained with 5 s recycle delays were superimposable on those with 20 s recycle delay, but we cannot exclude the possibility of a small fraction of deuterons with much longer relaxation times.

For all T_{1Z} experiments the standard nonselective inversion recovery with quadrupole echo detection pulse sequence was used, $180_x-\tau-90_x-40\ \mu s-90_y-\tau_1-$ACQ, with a 16-step phase cycle to suppress artifacts. Adequate signal-to-noise ratios were obtained by accumulating 3500−4000 transients of 1024 complex data points for each of 10−12 relaxation delays, τ. The 90° pulse length was 1.6 μs, resulting in acceptable spectral coverage over the spectral width ±200 kHz. The preacquisition delay, τ_1, was varied so as to place a sampling point precisely at the top of the echo. In most experiments, a 40 μs delay between pulses was chosen to shift the echo well outside the spectrometer dead time. A few experiments performed with 20 μs delay showed that for $\tau_1 = 40\ \mu$s transverse relaxation caused no deleterious effects. Line shapes obtained for pulse spacings longer than 60 μs are strongly attenuated due to dipolar coupling with relaxing ^{14}N[27] and can therefore not be fit using procedures described in this paper. Temperature-dependent relaxation studies were performed for generations 2, 3, and 9. For generations 1, 5, and 7 only room temperature data were obtained. Since all recovery curves were multiexponential functions of the relaxation delay, delay values were chosen to uniformly sample intensity for both the shortest and the longest relaxation times in the experiment. The recycle delay (typically 2−5 s) was chosen to ensure more than 90% magnetization recovery for the slowest relaxing component.

For each sample, the full T_{1Z} experiment took from 2 to 3 days, depending on the temperature, required recycle delay, and the number of τ values. Over this long acquisition period, the relative error for total intensity in the spectrum due to electronic instabilities is estimated to be 10−15%. This limited the range of temperatures at which experiments could be performed with reasonable accuracy. At temperatures lower than 15 °C, the limiting factor was the long T_{1Z} (≥1 s) of secondary amide and deuterated tertiary amine groups. At temperatures above 55 °C, a prohibitively low signal-to-noise ratio was caused by the small fraction of rigid material for generations 2 and 9 and by long T_{1Z} values for terminal ammonium groups of generation 3.

A few complementary T_{1Q} experiments were performed for generations 3 and 9 to check consistency of the motional models used to analyze the T_{1Z} data. The broadband Jeener-Broekaert sequence[28,29] $90_x-2t-67.5\bar{y}-2t-45_y-t-45_y-\tau-45\bar{x}-40\ \mu s-90\bar{x}-\tau_1-$ACQ was used with a 32 step phase cycle, with the same experimental conditions as described above for T_{1Z} experiment. The t value, 12 μs, was chosen so as to achieve uniform excitation of quadrupole order across the frequency range from 5 to 35 kHz, covering most of the RND_3^+ powder pattern. The τ_1 delay was adjusted to obtain an acquisition point at the zero crossing for the imaginary signal component.

Data Processing. Data manipulations and simulations were performed on O2 Silicon Graphics workstations using the data visualization package PV-WAVE and a locally written simulation package, EXPRESS.[17,30] Exponential apodization, corresponding to 500 Hz Lorentzian broadening, was applied to the time domain signals. The data were then left shifted so that the first point occurred precisely at the top of the echo for T_{1Z} and at the first zero crossing for T_{1Q} signals. A frequency independent phase correction of 5−15° was used to minimize the signal in the out of phase channel. The relatively small residual asymmetry in the Fourier transformed spectra may arise from instrumental artifacts and second-order effects not eliminated by phase cycling. Prior to generating recovery curves from partially relaxed spectra, small baseline shifts were applied to ensure that the average baseline was exactly zero.

3. Data Fitting Procedures and Motional Models

Wide distributions of motional parameters are usual for glassy polymers and can in many cases account for nonexponential relaxation of overall Zeeman and quadrupolar polarization.[31] However, there is a growing awareness that phenomenological distribution functions used to parametrize relaxation of the total polarization are not adequate to account for orientational anisotropy of the relaxation times.[13,14,32] Instead, detailed insight into the microscopic dynamics can be obtained by fitting the anisotropy of observed relaxation times to specific motional models. A recent study[33] of microscopic dynamics in glassy poly(α-methylstyrene) illustrates the power of this approach.

For PAMAM dendrimer salts, the data fitting procedure is greatly complicated by overlapping powder patterns, but because different motional models have different patterns of anisotropy, it is still possible to obtain reliable values of motional rates for specific dendrimer sites. Thus, the observed multiexponential character of the recovery curves is assumed to originate from single-exponential contributions of overlapping spectral features:

$$M_\infty(\nu) - M_\tau(\nu) = \sum_{i=1}^{N} I^i_{\text{total}}(m^i_\infty(\nu) - m^i_0(\nu))e^{-\tau/T_{1Z}{}^i} = \sum_{i=1}^{N} I^i_{\text{total}}(m^i_\infty(\nu) - m^i_\tau(\nu)) \quad (1)$$

Here, $M(\nu)$ is the overall spectral signal intensity at frequency ν (with *maximum* intensity normalized to 1), $m(\nu)$ is the signal intensity of a contributing feature (with *integrated* intensity normalized to 1), and I_{total} is the weighting factor for each overlapping component. Subscript "τ" indicates the delay time, and the summation index "i" labels the spectral component. N is the number of spectral features overlapping at a particular frequency ν. For the present study, the following was approximately valid: $N = 1$ for $|\nu| > 110$ kHz (contribution only from R_2ND deuterons), $N = 2$ for $45 < |\nu| < 110$ kHz (contribution from R_2ND and R_3ND^+), and $N = 5$ for $|\nu| < 45$ kHz (rigid, glassy R_2ND, R_3ND^+, RND_3^+, a broad and a narrow isotropic component). In practice, low signal-to-noise ratio prevented accurate analysis of signal intensities for $|\nu| > 100$ kHz. We also found for adequate fits of recovery curves, two contributions from ammonium deuterons had to be included for frequencies in the interval $|\nu| < 45$ kHz, so in this spectral region $N = 6$ (see Appendix). The latter two contributions differ only in relaxation time and relative intensity; their line shapes are superimposable. The procedure used to fit recovery curves for frequencies between 45 and 110 kHz is described in section 4 below, while the more complicated procedure needed for frequencies inside RND_3^+ powder pattern ($|\nu| < 45$ kHz) is discussed in the Appendix.

Simulations for each $m_\tau{}^i$ were done by solving the stochastic Liouville equation for the time evolution of the density matrix of a single deuteron undergoing Markovian jumps among different sites according to specific motional models.[18] The computations were performed using EXPRESS,[17,30] a simulation package developed to calculate T_{1Z} and T_{1Q} relaxation time anisotropies. For each spectral component the motional model is defined by the orientations of deuteron principal axes system (PAS) of the electric field gradient tensor and the rates of instantaneous jumps between orientational sites. The rates, site populations, Euler angles describing site orientations, and principal axis values of quadrupole coupling parameters, $\chi = (e^2q_{zz}Q/h)$ and $\eta = (q_{xx} - q_{yy})/q_{zz}$, for each spectral feature can be varied in the simulations. The individually simulated spectral features were added (according to eq 1) with appropriate relative weights. The total line shapes were then multiplied by a factor, $f(\nu) = \nu_0{}^2/(\nu_0{}^2 + Q^2(\nu - \nu_0)^2)$, to correct for the finite bandwidth of the probe. The deuteron Larmor frequency was $\nu_0 = 46.06$ MHz, and the probe quality factor, $Q = 105$, was determined by fitting a powder pattern of perdeuterated polyethylene.

The experimental and simulated recovery curves were compared for several representative points on the line shape, which had good signal-to-noise ratios. The simulations were repeated until the smallest global difference was achieved between experimental and simulated recovery curves for all these points. Quoted error bounds on the rates of motion correspond to rates which noticeably increase the difference between experimental and simulated recovery curves. This unwieldy procedure was necessary in order to account for nonexponential anisotropic relaxation of overlapping powder patterns. Since for the whole T_{1Z} experiment each computation takes, on average, 20−40 min of CPU time on a SGI O2 workstation, the task of fitting the data for a several dendrimer generations at different temperatures is somewhat daunting.

Fortunately, much simplification is possible due to intrinsic physical properties of the system. For most deuterons, the motion is in the fast regime and the relevant jump rates have at most minor effects on the equilibrium line shapes. Thus, before invoking EXPRESS to analyze the recovery curves, deconvolution of the equilibrium spectra can be performed rapidly, as described previously,[18] to yield the quadrupole coupling parameters, librational angles and relative intensities for spectral features originating from R_2ND, R_3ND^+, and RND_3^+, groups. During the computationally intensive dynamic simulations, these parameters were held constant, and only the relevant motional rates were varied.

We found the model of planar libration on an arc provides an adequate description of deuteron relaxation for R_2ND and R_3ND^+ groups. The number of jump sites on the arc was fixed at six in order to reproduce previously analyzed line shapes[18] with minimum error and computation time. The site orientations were chosen to uniformly sample the libration arc between 0° and the maximum librational amplitude, ϕ_0. Equiprobable jumps among all six sites were allowed in the simula-

tions. The distribution of quadrupole coupling parameters was modeled only as a homogeneous Gaussian broadening of 7 kHz half-width, which was applied to all spectra after simulation. This broadening cannot reproduce the generation and temperature dependent intensities, skewed due to H-bond length distributions discussed previously,[18] and introduces small errors in simulated line shape intensities. These errors can be neglected in the present study because the resulting uncertainty in the motional rates lies within experimental error bounds. Thus, the introduction of additional variable simulation parameters is not warranted by the precision of the data.

Attempts to improve the fit by incorporating distributions of libration rates were completely unsuccessful. Rates which give the best overall fit for planar libration yield T_{1Z} values close to the minimum. If 10-fold slower rates are included in the distribution, the simulated relaxation times are not greatly affected. However, the slow rates introduce characteristic line shape distortions which are not observed experimentally. Including faster rates in the distribution yields relaxation time anisotropies significantly smaller than those observed experimentally. These simulations show that for spacers (RND_2) and branches (R_2ND^+), there can be at most a 2−3-fold distribution of librational correlation times about the values quoted below. It is then reasonable to assume that narrow rate distributions also suffice to characterize motion of the RND_3^+ groups as well. Strong support for this hypothesis is provided by the experimental data for G3 at high temperature. For example, at 55 °C, powder patterns for spacer and branch point deuterons have collapsed, and recovery curves for the remaining ND_3^+ powder pattern are well described by single-exponential functions. This would not be the case if there were a broad, continuous distribution of rotational jump rates. We conclude from these simulations that unlike most linear glassy polymers, the description of local motion in solid, almost monodisperse dendrimers by a broad continuous distribution of correlation times is inappropriate.

It is shown in the Appendix that, in most cases, there are two contributions to ND_3^+ relaxation, distinguished by 3-fold rotational jump rates which differ by a factor of 10. The quadrupole coupling parameters were assumed to be the same for both contributions. Although the possibility of different librational amplitudes and site populations for these deuterons cannot be ruled out, the broadened line shapes do not provide enough resolution to constitute experimental evidence. Small deviations between simulated line shape intensities and experimental values which were observed for some high-temperature data sets (at the shoulders of the RND_3^+ powder pattern) may be a result of this approximation.

The recovery curves were not very sensitive to changes in the rate of libration of the RND_3^+ symmetry axis. A weak dependence of the simulated equilibrium line shape on this parameter sets bounds on the order of 10^5-10^8 s^{-1} for this librational rate. So, in all simulations for ammonium deuterons the rate of their C_{3v} axis libration was fixed at the average value, $k_c = 10^6$ jumps/s. Including the axis motion in the simulation results in approximately 1−2 kHz broadening of the line shape. Thus, Gaussian apodization of these simulated spectra was approximately 2 kHz smaller than when the motion was assumed to be fast.[18]

For RND_3^+ groups, a few simulations of the anisotropic quadrupole order relaxation time, T_{1Q}, were performed. The ammonium groups contribute most to the intensity in the frequency range excited under the experimental conditions described. These were used as a check on the validity of the motional model employed in T_{1Z} simulations (see Appendix). T_{1Q} data are known to be more sensitive to the presence of distributions of rates and slow motion.[17,30] Full deconvolution of multiexponential T_{1Q} recovery curves would require taking into consideration the excitation profile and line shapes distortions due to slow motion of the C_{3v} symmetry axes, in addition to contributions from underlying powder patterns. In light of the number of fit parameters required this task was deemed too complicated. But for some data sets, the difference in T_{1Q} of underlying powder patterns and ammonium deuterons was large enough to allow a biexponential fit to two effective T_{1Q} contributions, one coming predominantly from RND_3^+ groups and the other from underlying powder patterns. This allowed direct comparison to the T_{1Q} anisotropy results of EXPRESS simulations (see Appendix). Adequate fits of T_{1Q} anisotropies for ND_3^+ required the presence of a large excess population at one of the four librational sites, which consequently was fixed at 0.91 in all simulations. If site-dependent PAS quadrupole coupling parameters were used as well, the differences in populations of these sites would be much lower. Other fit parameters were the same as in corresponding T_{1Z} simulations.

4. Results and Discussion

Simulating recovery curves has to be done separately for each of the spectral components overlapping in a certain frequency range, followed by adding the contributions according to eq 1. The best signal-to-noise ratios are observed in the frequency range $|\nu| < 45$ kHz, but in this region it is difficult to analyze the recovery curves without any constraints due to the large number of overlapping components. Here, knowledge about relaxation anisotropies of the underlying spectral components is essential. It is important to realize that the total contribution to the apparent relaxation time at any given frequency will depend on the relative weights of each spectral component at this frequency, so the nature of the "effective" anisotropy is difficult to predict a priori. From EXPRESS simulations, we can calculate the T_{1Z} anisotropy of each of the components, using nonlinear regression (three parameter) fits to single-exponential functions. Simulations for the models of planar libration (R_2ND and R_3ND^+) and isotropic motion (mobile components) show that T_{1Z} values of the underlying spectral features do not vary substantially across the middle of the spectrum.

Since only two overlapping components (from spacer and branching sites) are observed in the range $|\nu| > 45$ kHz, it is reasonable to start the relaxation analysis in that region, even though the experimental errors are larger there. Information provided by the spectra in this range should be enough to determine the relaxation time anisotropies of secondary amide and deuterated tertiary amine sites. For many frequency points only two parameters are varied in these fits: the rates of librational motion at each of the two chemically distinct sites. The relative intensities of two components are fixed from static line shape simulations.[18]

Experimental recovery curves for generations 1, 3, and 5 are shown for two representative frequencies, 50

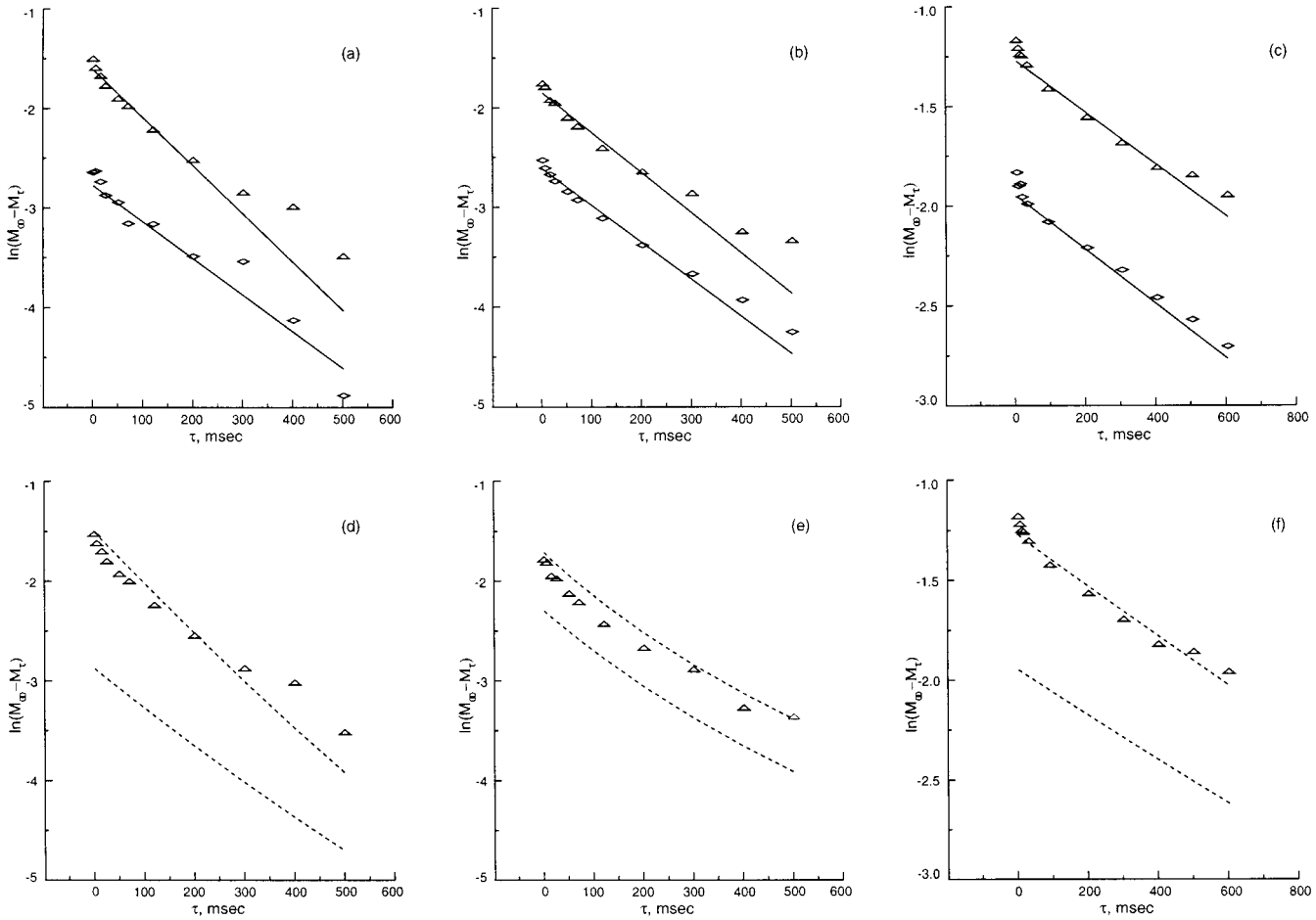

Figure 1. Room-temperature experimental recovery curves: (a, d) G1, (b, e) G2, and (c, f) G3 at 50 kHz (triangles) and 80 kHz (diamonds). Solid lines in parts a−c represent a single-exponential fit to experimental data. The "effective" fit T_{1Z} values for G1: 272 ± 44 ms at 80 kHz, 206 ± 30 ms at 50 kHz; G3: 270 ± 26 ms at 80 kHz, 248 ± 36 ms at 50 kHz; G5: 739 ± 54 ms at 80 kHz, 767 ± 67 ms at 50 kHz. Dashed recovery curves in parts d−f are the results of EXPRESS simulation for two overlapping spectral features from R_2ND and R_3ND^+ deuterons at 50 kHz (upper) and 5 kHz (lower). See Tables 1−3 for corresponding fit parameters.

kHz (triangles) and 80 kHz (diamonds), in Figure 1, parts a, b, and c, respectively. At 50 kHz the predominant intensity comes from R_3ND^+, and at 80 kHz it comes from R_2ND deuterons. Single-exponential functions (solid lines) turn out to be reasonable approximations for the relaxation at these frequencies. However, Figure 1, parts d, e, and f show that nonlinearity of the semilog recovery curves is better approximated by fitting to a weighted sum of exponentials (dashed lines), according to eq 1, especially for generation 3. Parts d, e, and f of Figure 1 also show nonexponential recovery curves simulated for R_3ND^+ deuterons near the middle of the spectrum (5 kHz, no symbols), using the same parameters which reproduce the experimental data at 50 kHz (triangles). This information is useful for deconvoluting the experimental recovery curves in this spectral region.

The above considerations suggest that an easy way to visualize the accuracy of the fit for the outer powder patterns is to simply compare anisotropies resulting from single-exponential fits to experimental data with the same procedure applied to simulated two-component recovery curves. Such a comparison, for generations 2, 3, and 9 at three representative temperatures, is shown in Figure 2. Similar fits have been performed for other temperatures and generations, but are omitted for brevity.

It is important to appreciate that the error bars shown for experimental data (symbols) come not only from finite signal-to-noise, but also from trying to fit two-component data to a single exponential. Nevertheless, this picture illustrates the level of detail and the accuracy of the information we can extract from relaxation at interior dendrimer sites.

Deuteron relaxation at spacer (R_2ND) and branching (R_3ND^+) sites gets faster with increasing temperature for all generations as illustrated in Figure 2. This observation can only be valid if the corresponding libration rates are on the slow side of the T_{1Z} minimum. The best fit rates of libration range from $k_l = 10^6-10^8$ s^{-1}. For the branching R_3ND^+ sites of generation 2 at 55 °C, adequately short T_{1Z} values (50 ms) can only be achieved in simulations using the kinetic model of equiprobable jumps among all sites and the rate of libration close to the T_{1Z} minimum ($k_l \sim 10^8$ s^{-1}). With exchange between nearest neighbors on a chain, the minimum achievable T_{1Z} is inadequate (70 ms). However, this observation does not conclusively validate the all-sites model. Neither model includes the possibility of contributions to relaxation from fluctuating intermolecular field gradients, arising from the motion of nearby chloride ions. Such effects should be considerably larger for R_3ND^+ than for R_2ND deuterons.

For secondary amide sites, the experimental data do not distinguish between all-sites and nearest neighbor jump models. To reproduce the observed relaxation times for the nearest neighbor jumps, motion should occur at a rate more than order of magnitude higher

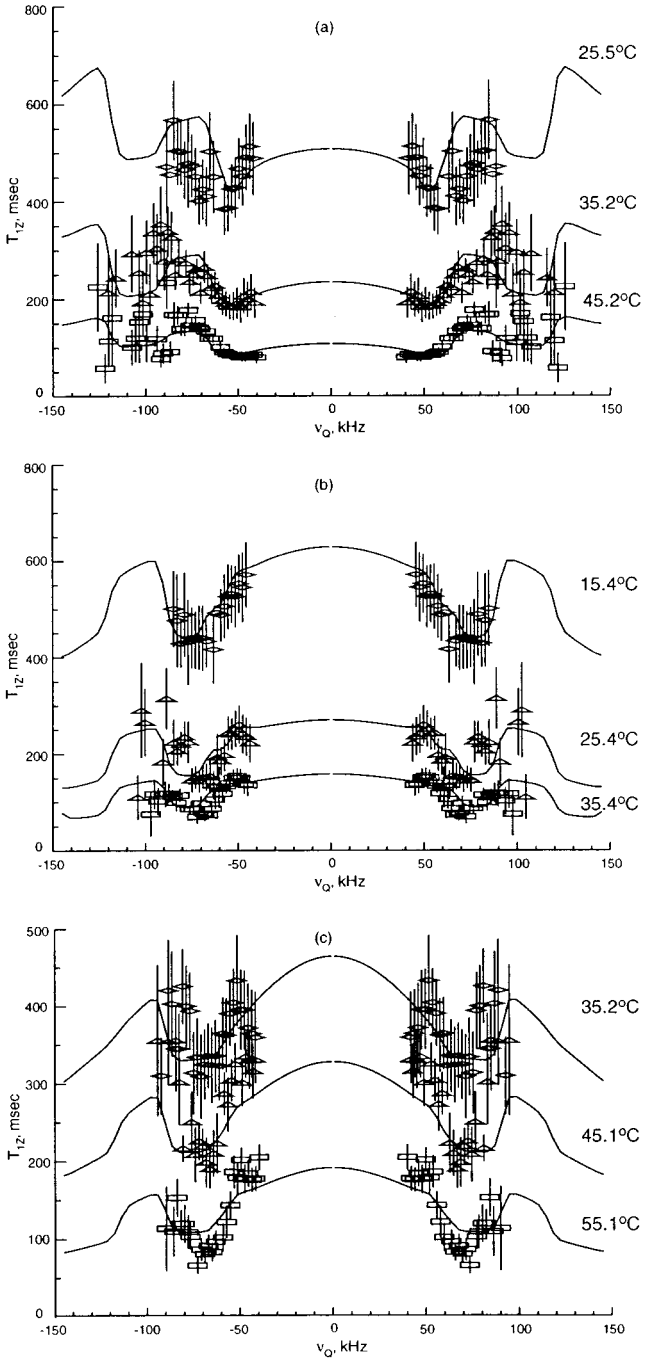

Figure 2. Comparison of single-exponential T_{1Z} fits for temperature-dependent experimental relaxation anisotropy data and EXPRESS simulations of overlapping R_2ND and R_3ND^+ powder patterns. Anisotropies are shown with temperature increasing from top to bottom: (a) G2 for $T = 25.5$, 35.2, and 45.2 °C; (b) G3 for $T = 15.4$, 25.4, and 35.4 °C; (c) G9 for $T = 35.2$, 45.1, and 55.1 °C.

than that for the all-site exchange model. However, the trends observed with changing temperature and generation number would be the same. Since the all-site model is required to describe branching site motion and an alkyl chain connects both sites in the same dendrimer molecule, we choose to adopt the all-site model for the secondary amide sites.

Best fit recovery curve simulations for underlying powder patterns were used as constraints when fitting recovery curves in the middle of the spectrum ($|\nu| < 45$ kHz). Here, four additional components have to be considered for adequate fits (see Appendix). Two of them

Table 1. EXPRESS Fit Parameters for R_2ND Groups of All Studied Dendrimer Generations

generation no., χ_{PAS} (kHz), η_{PAS}	$T \pm 0.05$ (°C)	I_{total}[b]	$\phi \pm 1$ (deg)	$k_l \times 10^6$ (s^{-1})
G1, 204, 0.12	25.40	18	13	3.4 ± 0.5
G2, 209, 0.12	25.45	32	17	0.7 ± 0.2
	35.15	21	19	0.9 ± 0.4
	45.15	10	19	2.0 ± 0.4
	55.15	4	21	3.9 ± 0.6
G3, 206, 0.12	15.40	15	17	1.1 ± 0.3
	25.40	22	18	2.5 ± 0.3
	35.40	15	18	4.9 ± 0.4
	45.40	7	18	5.4 ± 0.4
	55.40	0	...	...
G5, 209, 0.12	27.15	41	18	0.50 ± 0.05
G7, 209, 0.12	27.12	25	11	1.6 ± 0.3
G9, 210, 0.12	27.17[a]	31	11	1.9 ± 0.3
	35.15	33	14	1.6 ± 0.3
	45.12	34	17	2.0 ± 0.3
	55.14	24	17	4.4 ± 0.4

[a] A month after annealing at 55 °C for a day. [b] I_{total} is the integrated intensity of an R_2ND group. The total equilibrium spectrum, resulting from addition of all features (R_2ND, R_3ND^+, RND_3^+, Gaussian and Lorentzian), is normalized to unity at its highest point. The estimated error in I_{total} is ±20% of the quoted value.

Table 2. EXPRESS Fit Parameters for R_3ND^+ Groups of All Studied Dendrimer Generations

generation no., χ_{PAS} (kHz), η_{PAS}	$T \pm 0.05$ (°C)	I_{total}[b]	$\phi \pm 1$ (deg)	$k_l \times 10^6$ (s^{-1})
G1, 162, 0.05	25.40	18	15	4.3 ± 0.5
G2, 162, 0.05	25.45	8	11	11 ± 2
	35.15	14	11	15 ± 3
	45.15	7	11	50 ± 5
	55.15	3	11	100 ± 30
G3, 171, 0.05	15.40	8	18	0.7 ± 0.1
	25.40	10	19	0.9 ± 0.2
	35.40	10	19	1.7 ± 0.3
	45.40	5	20	2.1 ± 0.4
	55.40	0	...	...
G5, 159, 0.05	27.15	14	14	0.9 ± 0.1
G7, 162, 0.05	27.12	21	14	1.4 ± 0.2
G9, 159, 0.05	27.17[a]	23	11	3.7 ± 0.2
	35.15	14	11	3.3 ± 0.3
	45.12	17	11	3.9 ± 0.3
	55.14	20	14	4.6 ± 0.4

[a] A month after annealing at 55 °C for a day. [b] I_{total} is calculated for R_3ND^+ groups as indicated in the caption to Table 1. The estimated error in I_{total} is ±20% of the quoted value.

originate from mobile parts of the sample, and are best fit using orientation independent relaxation times of 10 ms for all temperatures and generations. Two others arise from RND_3^+ deuterons, with substantially different rates for 3-fold rotational motion. The details of the fit procedure and supporting considerations are described in the Appendix. Best fit parameters obtained for all generations and temperatures are summarized in Tables 1−4.

The tabulated total intensities, I_{total}, were calculated for the best fit equilibrium spectrum of the contributing feature, normalized to the maximum intensity of superposition spectrum. Such a representation is more meaningful for spectral simulations and comparison with experimental results. If necessary, the corresponding relative intensities can readily be estimated from these data. Error bounds on PAS values of quadrupole coupling parameters are the same as cited in ref 18.

The appearance of narrow peaks in the middle of the spectrum is associated with the onset of the glass transition, as described in ref 18. DSC measurements[18]

Table 3. EXPRESS Fit Parameters for RND_3^+ Groups of All Studied Dendrimer Generations

G no.[d]	T ± 0.05 (°C)	I_{total}[b]	β_c ± 2 (deg)	$p_3(\Omega(240°, \beta_c, 0°))$[c]	fraction "fast" ± 5 (%)	$k_3 \times 10^{10}$ (s^{-1}) "fast"	(k_3 ± 0.2) × 10^9 (s^{-1}) "slow"
G1	25.40	68	28	0.348	30	1.8 ± 0.2	1.3
G2	25.45	67	31	0.350	20	1.1 ± 0.3	1.1
	35.15	56	35	0.350	10	1.7 ± 0.5	1.1
	45.15	18	42	0.346	0	...	1.1
	55.15	7	50	0.348	0	...	1.1
G3	15.40	81	20	0.352	45	1.3 ± 0.2	1.3
	25.40	73	20	0.352	52	2.0 ± 0.2	1.3
	35.40	64	23	0.346	60	2.7 ± 0.3	1.3
	45.40	45	23	0.346	85	3.0 ± 0.3	1.3
	55.40	9	22	0.348	100	3.7 ± 0.2	
G5	27.15	76	25	0.350	20	1.9 ± 0.4	1.3
G7	27.12	76	25	0.350	15	1.3 ± 0.5	1.2
	27.17[a]	72	32	0.350	0	...	1.2
	35.15	77	32	0.350	10	1.1 ± 0.4	1.1
	45.12	73	36	0.346	0	...	1.2
	55.14	57	45	0.346	0	...	1.2

[a] A month after annealing at 55 °C for a day. [b] I_{total} is calculated for RND_3^+ groups as indicated in the caption to Table 1. The estimated error in I_{total} is ±10% of the quoted value. [c] $p_1 = p_2 = (1 - p_3)/2$; p_3 ± 0.001. [d] $\chi_{PAS} = 165$; $\eta_{PAS} = 0.06$.

Table 4. Integrated Fit Intensities of Lorentzian and Gaussian Components for All Studied Dendrimer Generations

generation no.	T ± 0.05 (°C)	I_{total}[a] (Gaussian)	I_{total}[a] (Lorentzian)
G1	25.40	25	1.3
G2	25.45	18	0.5
	35.15	12	9.7
	45.15	4	12.2
	55.15	0	14.8
G3	15.40	9	0.5
	25.40	19	0.6
	35.40	21	4.1
	45.40	19	8.0
	55.40	0	14.0
G5	27.15	18	0.5
G7	27.12	15	0.0
G9	27.17[a]	24	0.0
	35.15	13	0.0
	45.12	16	0.0
	55.14	19	1.9

[a] A month after annealing at 55 °C for a day. [b] I_{total} is calculated for Gaussian and Lorentzian components as indicated in the caption to Table 1. The estimated errors in I_{total} are ±10% of the quoted value for Gaussian components, and ±5% for Lorentzian components. The half-width of Gaussian and Lorentzian components were fixed to 14 kHz and 2 kHz, respectively, for all generations.

show that for G2 the transition starts near room temperature. The fact that both Gaussian and Lorentzian components appear in appreciable amounts at higher temperatures for high generation materials is consistent with their higher T_g. A similar increase of T_g with generation number has been observed for amine-terminated PAMAM dendrimers.[34] It is likely that rapidly tumbling residual solvent contributes some intensity to the central features at high temperature. Proton MAS spectra (data not shown), obtained at room temperature on the deuterated G2 sample several months after the deuteron relaxation measurements reported here, show that the contribution of residual solvent is less than 2% of the total spectral intensity. For all generations, the total intensity of the Gaussian component, which decreases from <10% at +15 °C to <1% at −30 °C, suggests that residual solvent may exert a plasticizing effect below T_g. However, for many glassy polymers, local large amplitude motion can produce a narrow NMR line shape component well below the onset of the glass transition as determined by DSC, even when there is no residual solvent.[31] The Lorentzian component, which appears only at temperatures well into the glass transition region, may be assigned to molten material.

Representative fits for generations 2, 3, and 9 at 35 °C, are shown in Figure 3, parts a, c, and e, together with deconvoluted single-exponential anisotropies from contributing deuterons, in Figure 3, parts b, d, and f. The amount of information obtained from these fits is appreciable.

From the data presented in Tables 1−3 and Figure 3, it can be seen that the relaxation times of R_3ND^+ deuterons at 35 °C increase monotonically with increasing generation, while the relaxation times of R_2ND deuterons pass through a minimum around G3. Relaxation times of the fast rotating fraction of RND_3^+ groups pass through a maximum at G3, while the relaxation times of slow rotating RND_3^+ groups are essentially independent of generation.

For librational motion, the relaxation time must decrease as the libration amplitude increases, and on the slow side of the T_{1Z} minimum it will decrease with increasing libration rate. Perusal of Tables 1−3 shows that the trends illustrated in Figure 3 reflect changes predominantly in libration rate rather than amplitude. For example, the large almost 4-fold increase in R_3ND^+ relaxation time for generation 3 and higher (compared to 100 ms for G2) is due to an approximately 10 fold decrease in libration rate at the branching sites. Simultaneously, the libration rate of spacer R_2ND groups passes through a maximum at $G = 3$, decreasing to a relaxation time of about 80 ms at 35 °C.

For identical motional parameters, libration-induced relaxation of R_2ND deuterons would be faster than that of R_3ND^+ deuterons by the square of the ratio of their corresponding quadrupole coupling constants (1.6). However, for generation 2 the R_2ND deuterons are observed to relax approximately 2.9 times slower than R_3ND^+ deuterons. Since the librational amplitudes are nearly the same, this difference can only be due to the much faster libration rate of the R_3ND^+ deuterons. This trend is reversed for the spacers and branching points of higher generations, where the spacer secondary amide deuterons relax faster (3 times for G3 and 1.3 times for G9) than those at the branching sites, and the librational rates at both sites are more nearly equal.

Although the data do not permit highly accurate determination of the rates of slow libration of the ammonium symmetry axis, the values used in simulations are comparable to the rates of libration at the secondary amide of the dendrimer interior. This suggests a possible correlation of librational motions at both sites, presumably mediated by the bonds of the dendrimer arms. If this is true, then it is far from obvious why the librational rates at R_2ND and R_3ND^+ sites are so different; they only are separated by a pair of methylene groups. As mentioned previously, one possibility is that the electric field gradient tensor of R_3ND^+ deuterons is determined, in part, by nearby chloride ions. Anion motion would then contribute to an apparent "libration" of these sites. If this is indeed the case, then the large values of apparent libration rate observed for R_3ND^+ in generations lower than 3 are simply a consequence of increased anion mobility in the

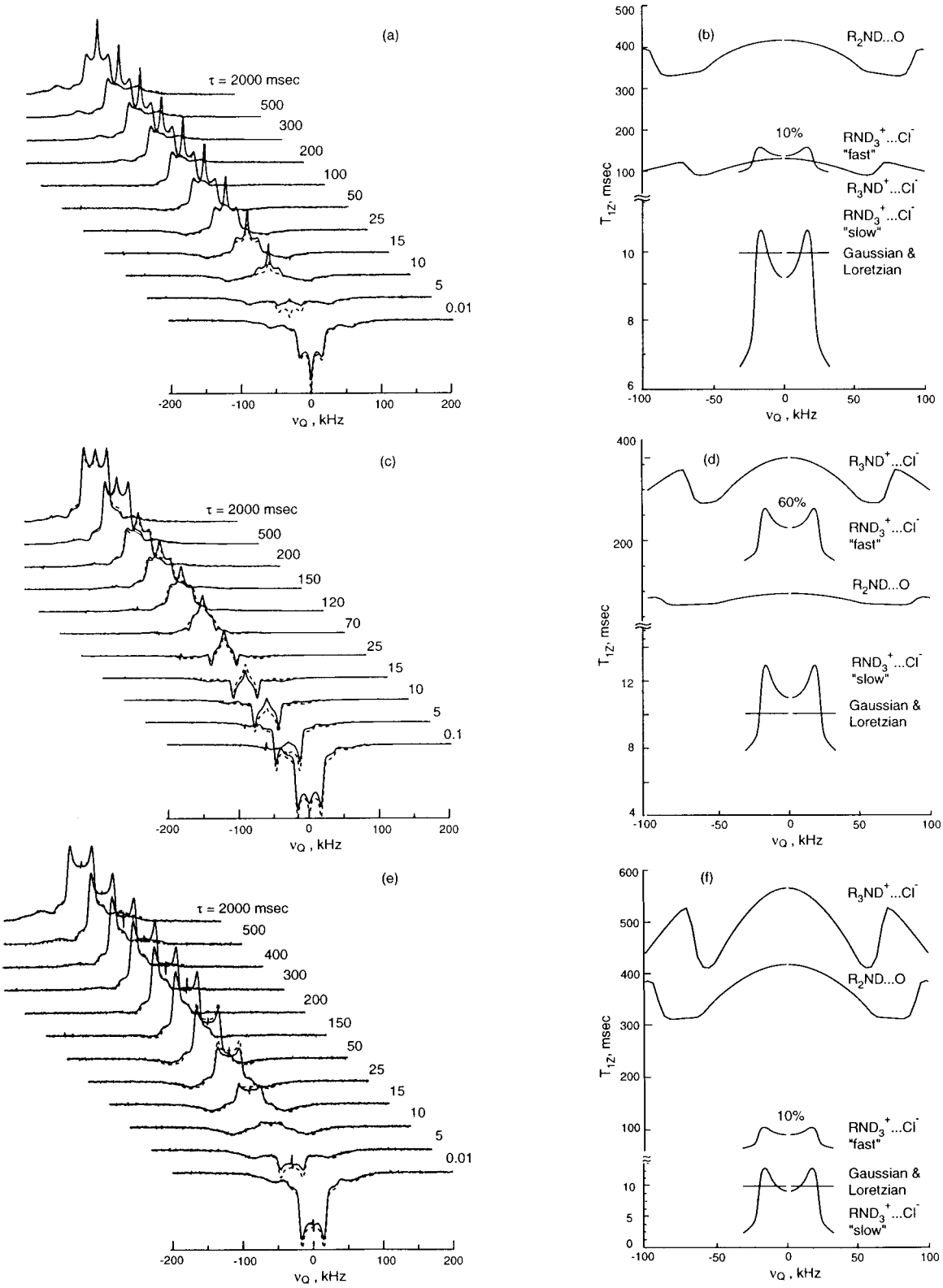

Figure 3. T_{1Z} experimental line shapes (solid lines) and overall fit (dashed lines) from EXPRESS simulation for (a) G2, (c) G3, and (e) G9 at 35 °C. Corresponding delay values, τ (ms), are listed to the right of the spectra. The derived relaxation time anisotropies of each contributing deuteron is shown in (b) G2, (d) G3, and (f) G9 (Notice the change in T_{1Z} scale around 100 ms). The fraction of fast ammonium rotors, RND_3^+, is 10 ± 5% for G2 and G9 and 60 ± 5% for G3 at this temperature (see Tables 1−3 for fit parameters).

more open structure of low generation materials.

The observation of similar libration rates of spacer R_2ND deuterons for low ($G = 2$, 3) and high ($G = 9$) dendrimers at any given temperature implies that the dendrimer arms in both environments experience similar constraints. This agrees with the expectation that high generation materials are extensively backfolded while low generation dendrimers are not.[4,9,19,35] The similarity of R_2ND librational rates therefore suggests that structure(s) associated with tangled, interpenetrated dendrimer arms belonging to different molecules in low generation materials resemble those of back-

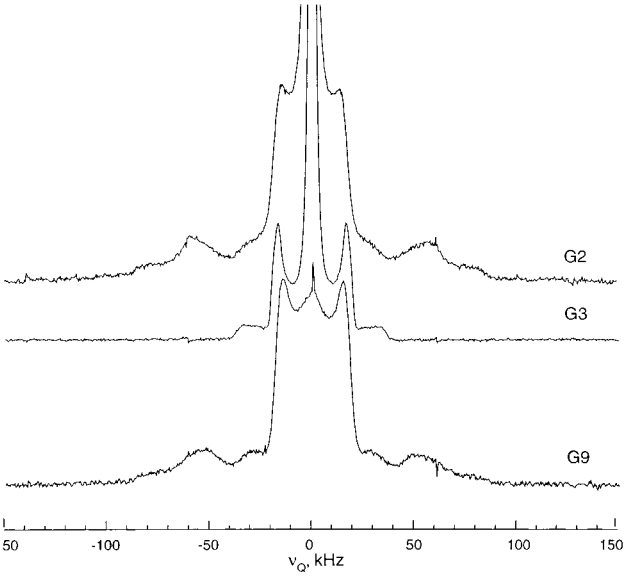

Figure 4. Experimental spectra of G2, G3, and G9 at 55 °C with 5 s recycle time. Notice the absence of outer powder patterns for G3.

folded, high generation dendrimers. For generation 3, the onset of backfolding reduces the extent of intermolecular penetration and leads to an increase in libration rate. This picture, suggested previously,[18] is also consistent with the maximum in libration amplitude of R_3ND^+ sites for G3 (see Table 2).

For G3 the fraction of fast ND_3^+ rotors increases with temperature, and approaches 100% at 55 °C. However, this fraction remains small for all other generations, and decreases rapidly with increasing temperature for both G2 and G9. A key to understanding this unusual behavior is the observation that, for both G2 and G9, the fraction of fast rotating RND_3^+ groups exhibits thermal hysteresis: e.g. a month after annealing G9 for a day above 55 °C, the fraction drops below the limit of detectability (~3−5%, see Appendix). We associate the fast rotating RND_3^+ groups with termini near the dendrimer surface. The thermal hysteresis observed for G2 and G9 (and to a lesser extent for G3) implies that some dendrimer arms are trapped in nonequilibrium configurations during solvent removal. For both G2 and G9, looser configurations which allow fast RND_3^+ rotation are thermodynamically less favored than more constrained, backfolded (high generation) or interpenetrated (low generation) configurations.

The intensity of the underlying R_3ND^+ and R_2ND powder patterns for G3 decrease rapidly with increasing temperature, and these features (as well as the contribution from the slow ammonium rotors) are completely absent from the 55 °C spectrum. This behavior is different from that of either G2 or G9 dendrimers, for which weak R_3ND^+ and R_2ND powder patterns are still evident at 55 °C (see Figure 4).

If the fast rotating ammonium groups are associated with less crowded environments near the dendrimer surface, the unique relaxation behavior of G3 suggests that there is an intermolecular network of weakly associated dendrimer arms, connected by more mobile branches. At 55 °C the amplitudes and rates of spacer motion in the mobile regions are sufficiently high to mimic essentially isotropic motion, so that all deuterons in such regions contribute only to the large central spike in the spectrum. We were able to model such behavior by allowing rotation about two C−C bonds in the ethylenediamine part of the spacer in addition to the libration of ND bond.

The network of termini is not stable for $G < 3$ because the dendrimer arms are too short, while for $G > 3$ globular (backfolded) structures are preferred. For G3 the fraction of RND_3^+ groups participating in the surface network can be estimated on the basis of the appropriate relative intensities. Analysis of integrated intensity data in Tables 1−4 shows that the increasing proportion of fast versus slow ammonium rotors with increasing temperature (Table 3) is actually due to a decrease in the intensity of slow component. In fact, this analysis suggests that the network of dendrimer termini, defined by the fast ammonium rotors, consists of a temperature independent fraction of 60−70% of all RND_3^+ groups. It is possible that such a fraction represents a "critical surface concentration", which allows intermolecular network formation without appreciable backfolding. The backfolded arms, associated with slowly rotating ammonium groups, apparently start to undergo a multiframe motion like the spacers surrounding them, completely averaging their quadrupole coupling tensors, and contribute intensity only to the central spike by 55 °C.

The slowly rotating ammonium deuteron component is associated with restricted environments caused by backfolding for high generations, interpenetration for low generations, and presumably both for generation 3. The fact that the rate of 3-fold jumps for these deuterons, $k_3 = (1.3 \pm 0.2) \times 10^9\ s^{-1}$, is independent of generation number (see Table 3) indicates that the nature of these constrained environments is the same for all PAMAM dendrimers. Its independence of temperature is very unusual behavior for 3-fold jumps and must be connected to the complexity of dendrimer structure. Phenomenologically, this can arise either from a collision frequency (preexponential factor) exponentially decreasing with temperature or an activation energy increasing linearly with temperature.

For the temperature range investigated, the Arrhenius plots for all deuterated sites of generation 2, 3, and 9 dendrimers are shown in Figure 5. The best fit Arrhenius activation parameters are summarized in Table 5. The activation energy for spacer R_2ND libration, $E_A = 44 \pm 5$ kJ/mol, is essentially independent of generation. It follows that the activation mechanism does not depend on whether the librating spacer units belong to interpenetrated or backfolded dendrimer arms. Independent of packing, the ND···O hydrogen bonding implies that two dendrimer arms are always involved in this motion. The relatively large amplitude libration in the dendrimer interior could break R_2ND···O hydrogen bonds, which accounts for the unusually large activation energy. The typical energies of hydrogen bonding are known to range from 20 to 40 kJ/mol[36] and depend on the donor−acceptor environment. Ordinarily, simple libration in the bottom of a potential would not be expected to exhibit a strong temperature dependence.[16]

The activation energy of "libration" at branching R_3ND^+ sites decreases with increasing dendrimer generation. It is larger than the activation energy of R_2ND sites for G2, almost equal for G3 and smaller for G9 (see Table 5). This supports the hypothesis that chloride ion motion modulates the R_3ND^+ electric field gradient tensor. If this picture is correct, activation energies derived from spin lattice relaxation of chloride ions

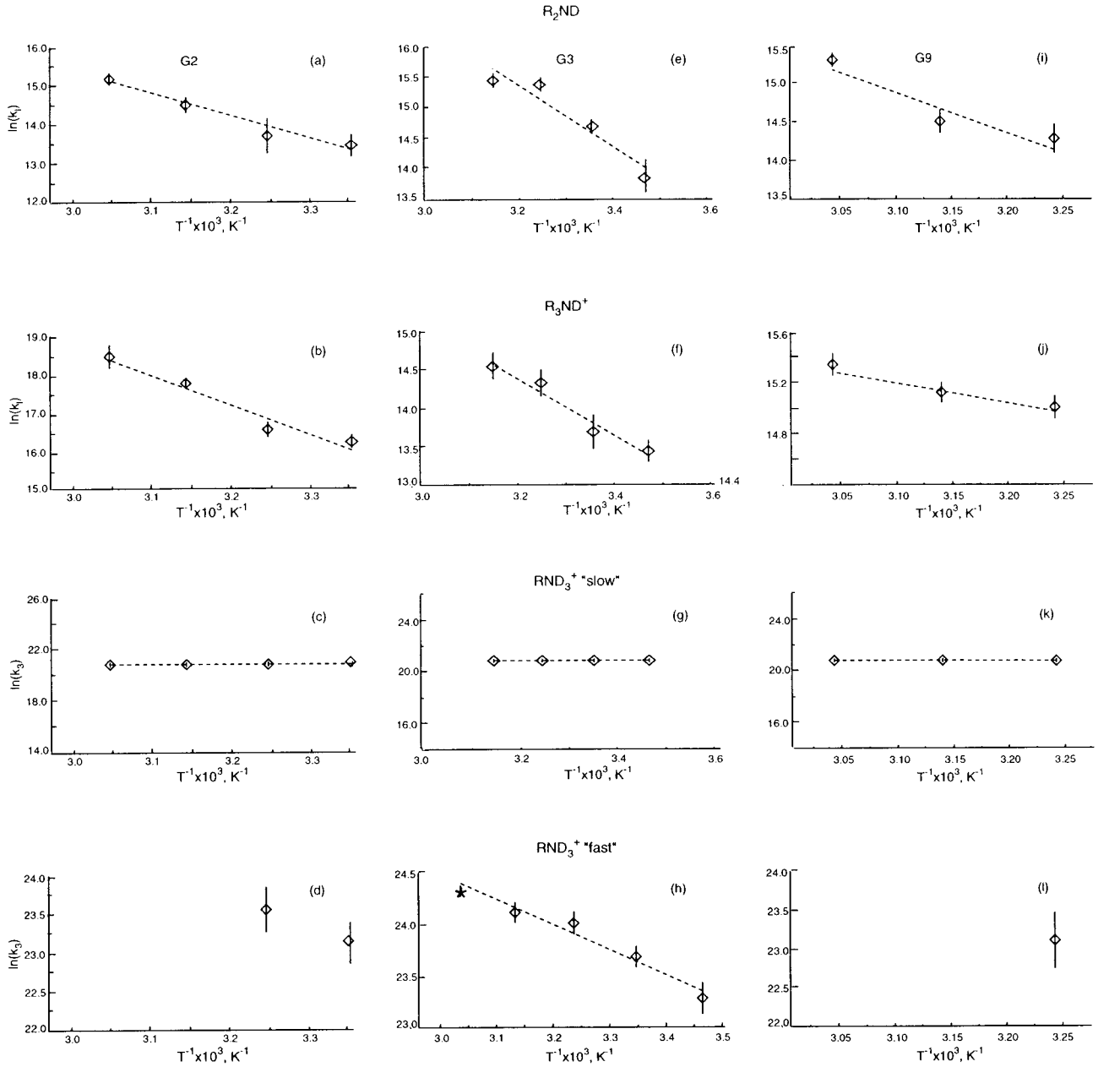

Figure 5. Temperature dependence of the rates of molecular motion (symbols) and Arrhenius fits (dashed lines) in (a−d) G2, (e−h) G3, and (i−l) G9. Contribution from fast RND_3^+ rotamers was not observed at all temperatures studied in (d) G2 and (l) G9 (corresponding symbols are missing). For G3 at 55.4 °C, the only contribution observed was from the fast RND_3^+ deuterons (star, h).

Table 5. Activation Energies, Logarithms of Collision Frequencies, and Rates of Motion for Generations 2, 3, and 9 PAMAM Dendrimers

group	G no.	E_A (kJ/mol)	ln(A)	k (s^{-1}) at 35 °C
R_2ND	G2	48 ± 7	33 ± 3	$(0.9 \pm 0.4) \times 10^6$
	G3	42 ± 8	28 ± 3	$(4.9 \pm 0.4) \times 10^6$
	G9	42 ± 10	31 ± 6	$(1.6 \pm 0.3) \times 10^6$
R_3ND^+	G2	64 ± 10	42 ± 4	$(1.5 \pm 0.3) \times 10^7$
	G3	30 ± 4	26 ± 2	$(1.7 \pm 0.3) \times 10^6$
	G9	14 ± 3	20 ± 1	$(3.3 \pm 0.3) \times 10^6$
RND_3^+, "fast"	G2	~30	~30	$(1.7 \pm 0.5) \times 10^{10}$
	G3	20 ± 2	32 ± 1	$(2.7 \pm 0.3) \times 10^{10}$
	G9	...	...	$(1.1 \pm 0.4) \times 10^{10}$

should follow the same trend as those of R_3ND^+ deuterons.

The hydrogen bond energy between charged atom pairs in salts is generally larger than between neutral atoms.[36] Therefore, the low activation energy at the branching sites of G9 suggests that hydrogen bonds between nitrogen and chlorine remain intact during librational motion. The motion of R_3ND^+ and Cl^- fragments could be "synchronized" by the highly constrained environment associated with backfolded arms of the dendrimer molecules. For generation 3, looser backfolding produces weaker constraints, allowing higher amplitudes of libration (Table 2) and presumably breaking of hydrogen bonds. On the other hand, since there is no appreciable interpenetration of neighboring molecules, the intermediate activation energy indicates that only one branch is involved. For generation 2, significant tangling between dendrimer molecules again hinders the motion, decreasing the librational amplitude (see Table 2), and almost doubling the activation energy (see Table 5). This could be due to the fact that breaking $R_3ND^+\cdots Cl^-$ hydrogen bonds now requires motion of two branches belonging to different dendrimer molecules.

For $R_2ND\cdots O$ hydrogen bonds two spacer units are always involved, since the trans conformation dominance for amide bonds prevents hydrogen bond formation within a single spacer.

The activation energy of the fast ammonium deuterons could be accurately determined only for G3. Our value is in agreement with the lower limit for crystalline ammonium salts cited in the literature.[23,24,37−39] This confirms the suggestion of a relatively unconstrained environment for fast RND_3^+ groups. The slight increase in activation energy of fast ammonium rotors for G2, with concomitant decrease in their fraction, is consistent with the generic picture of more constrained environments for interpenetrated low generation dendrimers.

5. Conclusions

Multiexponential deuteron relaxation behavior of PAMAM salts has been analyzed as a sum of contributions from branching R_3ND^+, spacer R_2ND, and terminal RND_3^+ deuterated sites. The site geometry, rates, and activation energies of each motion have been determined for low and high generation dendrimers. Analysis of librational motion at the spacer R_2ND sites reveals similarities in the mobility of these sites for low and high generation molecules. This rather surprising result is ascribed to the stabilization of $ND\cdots O$ hydrogen bonds by interpenetration of extended dendrimer arms for low generation dendrimers and backfolding of arms for high generation materials. Librational motion involves breaking the hydrogen bonds between neighboring branches.

For R_3ND^+ deuterons, the analysis is complicated by fluctuating intermolecular field gradients arising from nearby chloride ions. Nevertheless, this motion is adequately modeled by orientational jumps among sites on an arc. For these sites, we believe that the observed decrease in activation energy with increasing generation number is due to a decrease in the probability of breaking hydrogen bonds between ND^+ groups and nearby Cl^- ions. This is consistent both with intramolecular backfolding for high generation dendrimers and interpenetration of neighboring molecules for $G < 3$.

Two fractions of rotating RND_3^+ groups, distinguished by approximately 10-fold different rotation rates, are found for all dendrimer generations. The fact that both fractions are observed for all generations again supports the idea that the local environment of extensively interpenetrated arms of low generation dendrimers is similar to that of backfolded arms of high generation materials. The unique behavior of motional parameters for G3 indicates that, in the solid, its configurations and internal dynamics are determined by a nearly equal balance between intramolecular backfolding and intermolecular association of extended dendrimer arms. The latter allows relatively stable intermolecular surface networks to form in solid dendrimers.

Results reported here are in agreement with molecular dynamics simulations,[4] which predict a structural transition to a more compact backfolded architecture for dendrimer generations $G \geq 3$. On the other hand, we have found no indication of dense shell formation in solid dendrimers of either low or high generations, which is more consistent with a kinetic model.[20] Simulations reported here reveal different environments for surface and constrained termini, which is especially well pronounced for the "transition" generation G3. Such transition generations, being capable of surface network formation, might be more effective as sequestering agents.[40] Better quantitative characterization of libration of the dendrimer termini in the surface network could be achieved by deuteron magic angle spinning experiments, which are particularly sensitive to motions in kinetic window of interest, $k_l = 10^5-10^8$ s^{-1}.

Analysis of spin relaxation time anisotropies confirms the presence of extensive hydrogen-bonding network, as indicated by our previous work.[18] However, static line shapes[18] do not unambiguously distinguish intramolecular from intermolecular association of the secondary amide spacer units. Intra- and intermolecular hydrogen bonding and dynamics have been found to be similar at spacer sites of low and high generation materials. The extent of intermolecular hydrogen bonding can be better quantified by REDOR experiments on mixtures of specifically labeled materials of low and high generations. Such experiments have the benefit of providing more quantitative information on the H-bonding length, although preliminary estimations suggest that the experiments will push the edge of sensitivity due to long distances and effects of molecular motion.

The study of dynamics at branching R_3ND^+ sites reveals generation dependent contributions from fluctuating electric field gradient tensors of nearby chloride anions. In general, the anions act to increase relaxation efficiency. Therefore, such materials may be useful for imaging applications,[41] where increasing relaxivity of medium with contrasting agents is an issue.

In distinct contrast to solution studies,[2,3] narrow distributions of structural and dynamic parameters are observed in solid dendrimers for all generations. Despite the tendency of low generation dendrimers to adopt open, quasi-planar structures in solution, the rates and amplitudes of local segmental motion in solid dendrimers are very similar for low and high generation materials. This implies that dynamic constraints on highly backfolded arms in high generation dendrimers are very similar to those found for strongly interpenetrated arms in low generation materials.

Acknowledgment. This work was supported in part by National Science Foundation grants CHE 9701014 and DMR9973933. The authors are grateful to the Michigan Molecular Institute (http://www.mmi.org/mmi/dendritech/pamam.html) for supplying G5, G7, and G9 materials for the present study and to Dr. Petar Dvornic (MMI) for helpful discussions.

Appendix: Relaxation Time Anisotropies of Multiple Overlapping Powder Patterns

Typical recovery curves obtained at 25 °C for G3 PAMAM dendrimers, at three frequencies within the boundaries of the RND_3^+ powder pattern, are shown in Figure 6. The solid lines represent best fits to experimental data (symbols), obtained by procedures described below. We note in passing that for some dendrimers, at some temperatures, normalized recovery curves of this type can be fit reasonably well phenomenologically, using a biexponential function of the form: $A_f e^{-\tau/T_{1f}} + (1 - A_f)e^{-\tau/T_{1s}}$, where the subscripts f and s denote fast and slow, respectively. However, this procedure ignores the fact that, in the indicated frequency range, there are contributions from at least three powder patterns in addition to Gaussian and Lorentzian lines centered at zero frequency. Unconstrained fits to such multiexponential recovery curves, especially with limited signal-to-noise ratio, are notoriously unreliable. To avoid such difficulties, we take advantage of the fact that motional

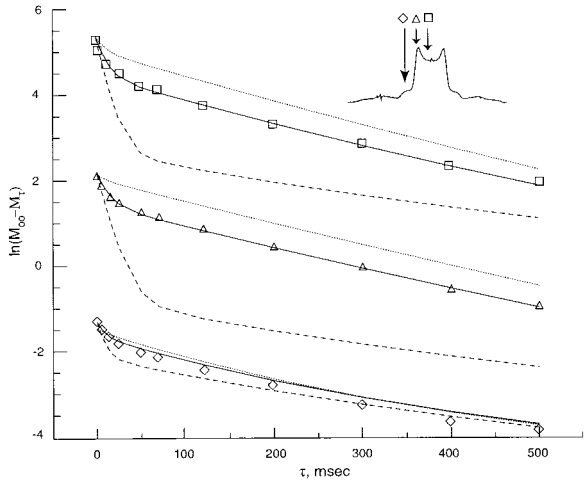

Figure 6. Experimental T_{1Z} recovery curves for ND_3^+ rotors of G3 at 25.4 °C (symbols). Recovery curves are shown at frequencies 36.3 kHz (diamonds), 16.4 kHz (triangles, shifted vertically by 1.5 for clarity), and 5.1 kHz (squares, shifted vertically by 5), and their corresponding position on the line shape is illustrated by the insert. Constrained multiexponential fits correspond to only slow (dashed lines), only fast (dotted lines), and both (solid lines) slow (48%) and fast (52%) ND_3^+ rotors.

models for each type of deuteron predict the anisotropy of the relaxation time, i.e., its orientation dependence, in terms of a limited number of parameters. Thus, the overall recovery curve at any frequency can be generated by summing contributions calculated for each spectral feature. Here, we show that even when underlying powder patterns contribute to the recovery curves, this approach can be used to obtain quantitative information about RND_3^+ motion.

Fitting the observed recovery curves was accomplished in stages. First, recovery curves for the underlying powder patterns for R_2ND and R_3ND^+ were computed in the frequency range $|\nu| \leq 45$ kHz. As described in the text, the rates and librational amplitudes used to generate these contributions were determined by fitting data *outside* this interval, and were not further adjusted. Next, the contributions from the central features were estimated by performing unconstrained, biexponential fits to experimental data for frequencies in the range $|\nu| \leq 5$ kHz. It was found that the "fast" time constant for these recovery curves was isotropic (orientation independent) and temperature independent, approximately equal to 10 ms for all dendrimer generations. Recovery curves with this time constant, generated for Gaussian and Lorentzian central features, were added to the recovery curves computed for R_2ND and R_3ND^+ powder patterns. The relative weight assigned to these contributions was fixed by independent fitting of equilibrium spectra as described in ref 18. Then recovery curves for RND_3^+ powder patterns were generated based on the two-frame model of (rapid) 3-fold jumps combined with (slower) jumps of the 3-fold jump axis among four sites defining a cone. The results were added to the fixed contributions from the other spectral components and compared with experimental recovery curves. These simulations, as well as those for librational motion of the R_2ND and R_3ND^+ groups, were all done by solving the stochastic Liouville equation using EXPRESS.[17,30] This time-consuming calculation was necessary because even though the 3-fold jumps are fast, libration of the 3-fold axis is not. The calculations confirm that while T_{1Z} is determined primarily by the 3-fold jump rate, the line shape is dependent on all the site populations and the rate of the slow motional process. The latter parameters were fixed by fitting equilibrium line shapes. Thus, for purposes of simulating a RND_3^+ recovery curves, only one parameter remains adjustable: the 3-fold jump rate, k_3.

The dashed and dotted lines shown in Figure 6 were determined from simulated spectra obtained as functions of the relaxation delay by adding correctly weighted underlying contributions to simulated RND_3^+ powder patterns according to eq 1. The RND_3^+ jump rate for the dashed lines, $k_3 = 1.3 \times 10^9$ s^{-1}, was chosen to best match the short time behavior of the experimental recovery curves. However, these simulations fail to match the data for recovery times greater than 50−150 ms (depending on frequency). The dotted lines, with $k_3 = 2.0 \times 10^{10}$ s^{-1}, give the best slopes for long recovery times but fail to fit the short time behavior. These results demonstrate that no single value of k_3 can account for the observed recovery curves. The solid lines were obtained by adding a weighted sum of two different RND_3^+ contributions, with different values of k_3. Additional simulations (data not shown) indicate that comparable fits can be obtained using a continuous distribution of k_3 values, but only if the distribution is sharply bimodal with maxima near the two values used in Figure 6. We conclude that, for G3 at 25 °C, the data indicate the existence of two RND_3^+ environments, distinguishable by different 3-fold jump rates. Parameters obtained by this procedure for other temperatures and other dendrimer generations are summarized in Table 3 of the main text. The quoted error limits are qualitative estimates, based on visual comparison of simulated and experimental recovery curves as well as the computed sum of squares of deviations between calculated and experimental points.

The presence of ammonium groups with different relaxation behavior is also found for high and low generation dendrimers. For these materials, the fraction of slow ammonium rotors is large at most temperatures studied. A quite different picture was observed for G3: this is the only generation for which the fraction of fast ammonium rotors increases with increasing temperature. For instance, at 45 °C the fraction of slowly rotating ammonium groups was only 15%. In this case, an unconstrained biexponential fit procedure yields reliable values for T_{1Z} (slow). These are found to be in good agreement with a single component EXPRESS simulation for slowly relaxing fast ammonium rotors not only for T_{1Z} but also for T_{1Q} (Figure 7a). Single component comparison for RND_3^+ is likewise facilitated by the small fraction of intensity coming from fast relaxing underlying powder patterns at this temperature.

The experimental T_{1Q} values (the slow component from the biexponential fit) are slightly shorter than those predicted by single component simulations for fast ammonium rotors, due to contributions from the underlying powder patterns. The latter relaxation times are short at this temperature (see, e.g., Figure 4 in the main text), but the biexponential fitting procedure does not remove them completely from T_{1Q} (slow), thereby pulling down the apparent slow component. This effect is most pronounced on the shoulders of RND_3^+ T_{1Q} anisotropy, where the fraction of intensity from underlying powder patterns is still relatively high.

Room-temperature data obtained for G9 after annealing show a dominant contribution from slow ammonium

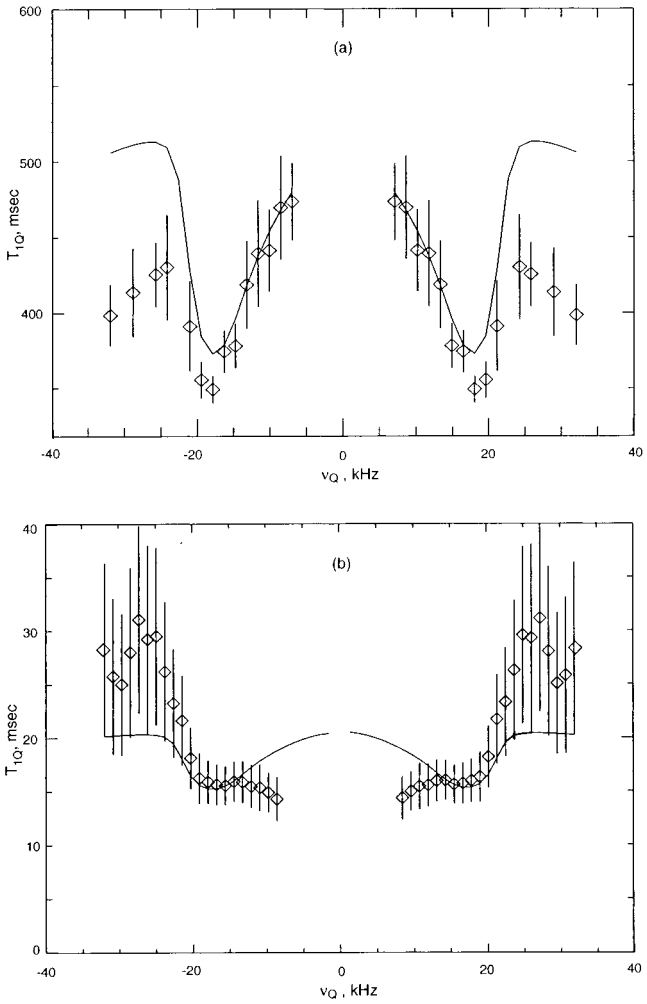

Figure 7. Single component experimental (symbols) and simulated (lines) T_{1Q} anisotropies for (a) G3 at 45 °C slow component and (b) G9 at 27 °C (a month after annealing at 55 °C) fast component. The motional parameters used were derived from T_{1Z} data and are listed in Table 3.

rotors (more than 95%). Once again, the fit for experimental T_{1Q} data (Figure 7b) can be compared with EXPRESS simulations, but in this case the fast relaxing component from biexponential fits to experimental data is used, since most of the contribution to the slowly relaxing component comes from the underlying powder patterns at this temperature. The fit is not as good as for G3 because the faction of underlying powder pattern intensities is high, and produces distortions in the biexponential fit, as reflected in the error bars. As expected, this effect is especially noticeable at the shoulders of the ammonium powder pattern (Figure 7b). In contrast to G3 data, the experimental values are now too long, because relaxation times for the underlying powder patterns are longer than for the ammonium groups (Figure 2). Despite these minor discrepancies, the general agreement between measured T_{1Q} anisotropies and those computed using parameters determined from the analysis of T_{1Z} data provides reassurance that the derived parameters do not suffer from serious systematic errors.

References and Notes

(1) Newkome, G. R.; Moorefield, C. N.; Voegtle, F. *Dendritic Molecules*; VCH Publishers: New York, 1996.

(2) Meltzer, A. D.; Tirrell, D. A.; Jones, A. A.; Inglefield, P. T. *Macromolecules* **1992**, *25*, 4549−4552.

(3) Meltzer, A. D.; Tirrell, D. A.; Jones, A. A.; Inglefield, P. T.; Hedstrand, D. M.; Tomalia, D. A. *Macromolecules* **1992**, *25*, 4541−4548.

(4) Naylor, A. M.; Goddard, W. A. I. *J. Am. Chem. Soc.* **1989**, *111*, 2339−2341.

(5) Moreno-Bondi, M. C.; Orellana, G.; Turro, N. J.; Tomalia, D. A. *Macromolecules* **1990**, *23*, 910.

(6) Ottaviani, F. M.; Bossmann, S.; Turro, N. J.; Tomalia, D. A. *J. Am. Chem. Soc.* **1994**, *116*, 661−671.

(7) Ottaviani, F. M.; Montani, F.; Turro, N. J.; Tomalia, D. A. *J. Phys. Chem. B* **1997**, *101*, 158−166.

(8) Gopidas, K. R.; Leheny, A. R.; Caminati, G.; Turro, N. J.; Tomalia, D. A. *J. Am. Chem. Soc.* **1991**, *113*, 7335−7342.

(9) Prosa, T. J.; Bauer, B. J.; Amis, E. J.; Tomalia, D. A.; Scherrenberg, R. *J. Polym. Sci., Part B: Polym. Phys.* **1997**, *35*, 2913−2924.

(10) Gao, Y.; Langley, K. I.; Karasz, F. E. *Macromolecules* **1992**, *25*, 4902−4904.

(11) Tomalia, D. A.; Baker, H.; Dewald, J.; Hall, M.; Kallos, G.; Martin, S.; Roeck, J.; Ryder, J.; Smith, P. *Macromolecules* **1986**, *19*, 2486.

(12) Spiess, H. W. *Colloid Polym. Sci.* **1983**, *261*, 193−209.

(13) Vold, R. R.; Vold, R. L. *Adv. Magn. Opt. Res.* **1991**, *16*, 85−171.

(14) Hoatson, G. L.; Vold, R. L. *NMR: Basic Princ. Prog.* **1994**, *32*, 1−61.

(15) Usha, M.; G.; Wittebort, R. J. *J. Mol. Biol.* **1989**, *208*, 669−678.

(16) Usha, M. G.; Peticolas, W. L.; Wittebort, R. J. *Biochemistry* **1991**, *30*, 3955−3962.

(17) Vold, R. L.; Hoatson, G. L.; Tse, T. Y. *Chem. Phys. Lett.* **1996**, *263*, 271−273.

(18) Malyarenko, D. I.; Vold, R. L.; Hoatson, G. L. *Macromolecules* **2000**, *33*, 1268−1279.

(19) Uppuluri, S.; Tomalia, D. A.; Dvornic, P. R. *Polym. Mater. Sci. Eng.* **1997**, *77*, 116−117.

(20) Lescanec, R. L.; Muthukumar, M. *Macromolecules* **1990**, *23*, 2280−2288.

(21) Morgan, D. R.; Stejskal, E. O.; Andrady, A. L. *Macromolecules* **1999**, *32*, 1897−1905.

(22) van Genderen, M. H. P.; Baars, M. W. P. L.; Elissan-Roman, C.; de Brabender-vanden Berg, E. M. M.; Meijer, E. W. *Polym. Mater. Sci. Eng.* **1995**, *73*, 336−337.

(23) Gruwel, M. L. H.; Wasylishen, R. E. *Z. Naturforsch.* **1991**, *46A*, 691−696.

(24) Gruwel, M. L. H.; Wasylishen, R. E. *Z. Naturforsch.* **1992**, *47A*, 1073−1086.

(25) Wasylishen, R. E.; Pettitt, B. A.; Dong, R. Y. *J. Chem. Soc., Faraday Trans. 2* **1980**, *76*, 571−573.

(26) Hunt, M. J.; Mackay, A. L. *J. Magn. Reson.* **1976**, *22*, 295−301.

(27) Heaton, N. J.; Vold, R. R.; Vold, R. L. *J. Chem. Phys.* **1989**, *91*, 56−62.

(28) Hoatson, G. L. *J. Magn. Reson.* **1991**, *94*, 152−159.

(29) Wimperis, S. *J. Magn. Reson.* **1990**, *86*, 46−55.

(30) Tse, T. Y. Ph.D. Dissertation, College of William and Mary, 1995.

(31) Bovey, F. A.; Mirau, P. A. *NMR of Polymers*; Academic Press: San Diego, CA, 1996.

(32) Griffin, R. G.; Beshah, K.; Ebelhauser, R.; Huang, T. H.; Olejniczak, E. T.; Rice, D. M.; Siminovitch, D. J.; Wittebort, R. J. *NATO ASI* **1988**, *C228*, 81−105.

(33) O'Conner, R. D.; Ginsburg, E. J.; Blum, F. D. *J. Chem. Phys.* **2000**, *112*, 7247−7259.

(34) Uppuluri, S.; Tomalia, D. A.; Dvornic, P. R. In *Polymeric Materials Encyclopedia*; Salamone, J. C., Ed.; CRC Press: New York, 1996; Vol. 3, pp 1824−1830.

(35) Amis, E. J.; Topp, A.; Bauer, B. J.; Tomalia, D. A. *Polym. Mater. Sci. Eng.* **1997**, *77*, 183−184.

(36) *Concise Encyclopedia Chemistry*; Jakubke, H.-D., Jechkeit, H., Eds.; Walter de Guyter: Berlin, New York, 1994.

(37) Ishida, H.; Ikeda, R.; Nakamura, D. *Bull. Chem. Soc. Jpn.* **1982**, *55*, 3116−3118.

(38) Ishida, H.; Ikeda, R.; Nakamura, D. *J. Phys. Chem.* **1982**, *86*, 1003−1008.

(39) Ishida, H.; Ikeda, R.; Nakamura, D. *Bull. Chem. Soc. Jpn.* **1986**, *59*, 915−924.

(40) Sayed-Sweet, Y.; Hedstrand, D. M.; Spinder, R.; Tomalia, D. A. *J. Mater. Chem.* **1997**, *7*, 1199−1205.

(41) Wiener, E. C.; Brechbiel, M. W.; Brothers, H.; Magin, R. L.; Gansow, O. A.; Tomalia, D. A.; Lauterbur, P. C. *Magn. Res. Med.* **1994**, *31*, 1−8.

MA000921U